# Copper Complexes Bearing Pendant, Protonatable Noncoordinating Groups: Synthesis, Characterization, and Protonation Chemistry

**Nydia D. Villanueva,[†] Michael Y. Chiang,[‡] and Jeffrey R. Bocarsly*,[†]**

Departments of Chemistry, The University of Connecticut, Storrs, Connecticut 06269, and National Sun Yat-Sen University, Kaohsiung, Taiwan 804, Republic of China

*Received April 4, 1997*

We have derivatized the pendant amine of (5-amino-5-methyl-3,7-diaza-2,9-nonanedioato)chlorocopper(II) with 3-pyridinecarboxaldehyde and 4-pyridinecarboxaldehyde. These new complexes, along with the starting material, comprise a set of copper complexes with chemically identical inner coordination spheres that provide protonatable nitrogen attached to the ligand framework. The 3-pyridinecarboxaldehyde adduct has been characterized by X-ray crystallography. This complex crystallized in the space group $P2_1/n$ with $a = 12.025(8)$ Å, $b = 12.304(5)$ Å, $c = 13.311(8)$ Å, $\beta = 94.76(5)°$, $V = 1962(1)$ Å$^3$, and $Z = 4$ ($R$, $R_w = 0.049$; 0.045). pH-dependent changes in the electronic spectroscopy and electrochemistry of these complexes have been observed. The parent complex undergoes a ∼300 cm$^{-1}$ shift in $\lambda_{max}$ and a +140 mV shift in midpoint potential on going from high pH to low pH, while the pyridinecarboxaldehyde Schiff-base derivatives undergo smaller changes (78 and 110 cm$^{-1}$ and 104 and 100 mV, respectively). The origins of the shift in $\lambda_{max}$ are investigated spectroscopically. A number of explanations for these shifts can be ruled out, including metal complex dimerization and axial coordination to the metal complexes. The data tend to support the suggestion that the spectroscopic shifts are largely due to the electrostatic influence of the pendant charge on the transition metal chromophore.

## Introduction

The electrostatic structure of molecules including the presence of intramolecular Coulombic interactions plays an influential role in determining the physical and chemical features of molecular systems.[1−3] There are relatively few simple model systems in which the effects of electrostatic perturbations on physical characteristics have been studied.[4−6] As an initial set of models for the presence of ionizable groups proximate to metal centers, we have derivatized (5-amino-5-methyl-3,7-diaza-2,9-nonanedioato)chlorocopper(II) (**1**)[7,8] (Chart 1), which contains a pendant amine, with 3-pyridinecarboxaldehyde and 4-pyridinecarboxaldehyde, to generate a set of complexes that have pendant protonatable sites (Chart 1). These complexes, along with their starting material, comprise a set of five-coordinate copper complexes with chemically identical inner coordination spheres that provide protonatable nitrogen atoms covalently attached to the ligand framework.

In the course of studying these complexes, we have observed pH-dependent changes in the electronic spectroscopy and electrochemistry. These pH-dependent phenomena may shed light on some of the fundamental physical effects of the presence of noncoordinating ionizable groups in metal complexes. In this study, we report the synthesis and structural characterization of the new complexes containing pendant protonatable nitrogen sites and the physical behavior of these complexes and their parent complex as a function of pH. Our interest is in characterizing the basis for the pH-dependent changes observed, as models for what may happen in metalloproteins when ionizable groups are found in close proximity to metalloprotein centers.

**Chart 1**

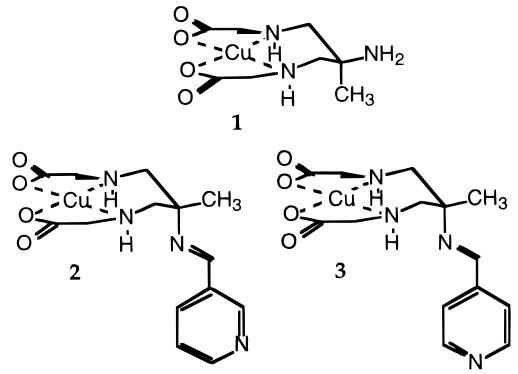


## Experimental Section

UV−vis spectra were recorded on an SLM-Aminco Milton-Roy 3000 diode array spectrophotometer. The positions of peak maxima were determined from the zero crossing of the first derivatives of the spectra. Infrared spectra were recorded as KBr pellets using a Midac M1200 FTIR spectrophotometer. NMR spectra were recorded on a Bruker DRX400 Avance spectrophotometer operating at 400.13 MHz. EPR

* To whom correspondence should be addressed.
† The University of Connecticut.
‡ National Sun Yat-Sen University.

(1) Honig, B.; Nicholls, A. *Science* **1995**, *268*, 1144.
(2) Sharp, K. A.; Honig, B. *Annu. Rev. Biophys. Chem.* **1990**, *19*, 301.
(3) Gunner, M. R.; Honig, B. *Proc. Natl. Acad. Sci. U.S.A.* **1991**, *88*, 9151.
(4) Bond, A. M.; Lawrance, G. A.; Lay, P. A.; Sargeson, A. M. *Inorg. Chem.* **1983**, *22*, 2010.
(5) Plenio, H.; Yang, J.; Diodone, R.; Heinze, J. *Inorg. Chem.* **1994**, *33*, 4098.
(6) Comba, P.; Curtis, N.; Lawrance, G. A.; Sargeson, A. M.; Skelton, B. W.; White, A. H. *Inorg. Chem.* **1986**, *25*, 4260.
(7) Comba, P.; Hambley, T. W.; Lawrance, G. A.; Martin, L. L.; Renold, P.; Varnagy, K. *J. Chem. Soc., Dalton Trans.* **1991**, 277.
(8) Balla, J.; Bernhardt, P. V.; Buglyo, P.; Comba, P.; Hambley, T. W.; Schmidlin, R.; Stebler, S.; Varnagy, K. *J. Chem. Soc., Dalton Trans.* **1993**, 1143.

S0020-1669(97)00384-4 CCC: $15.00 
Published on Web 02/04/1998

spectra were acquired on a Bruker X-band spectrophotometer (9.34 GHz) equipped with an Oxford cryostat at 12 K in 2:1 ethylene glycol−phosphate buffer solutions at 3 mM metal complex concentrations. Electrochemical experiments were performed on a BAS 100 electrochemical analyzer. pH titrations were performed using a Fisher Scientific pH meter. All materials were of reagent grade and were used without further purification unless otherwise noted.

**Synthesis of 1-H$^+$.** Complex **1-H**$^+$ was synthesized according to the literature procedure.[7] Free ligand from **1** was prepared according to the literature procedure[7] or by treatment of metal complex with excess $Na_2S$ in water, followed by treatment with decolorizing charcoal, filtration and evaporation to dryness.

**Synthesis of 1.** **1-H**$^+$ (1.06 g, 3.0 mmol) was slurried in water (60 mL). The pH of the solution was adjusted to 10.0 with a saturated solution of NaOH. Acetone (240 mL) was added slowly with stirring. The solution was then covered and allowed to stand overnight at room temperature. Microcrystalline solid precipitated during this time and was collected, washed with acetone, and allowed to air-dry. A 0.75 g quanity of product was collected (81%). Anal. Calcd for $C_8H_{15}N_3O_4Cu\cdot1.5H_2O$: C, 31.22; H, 5.89; N, 13.65. Found: C, 31.99; H, 5.87; N, 13.92.

**Synthesis of 2.** **1** (0.28 g, 0.91 mmol) was slurried in methanol (80 mL). Distilled 3-pyridinecarboxaldehyde (0.20 mL, 2.1 mmol) was added, and the solution was refluxed for 5 h. The reaction mixture was then allowed to cool, and its volume was reduced in vacuo. The solution was stored at room temperature for crystallization, after which the crystalline product was collected by filtration. Upon drying in the air, the crystalline product decomposed to a bright blue powder over several hours. 0.358 g of powdered product was collected after drying (90% yield). The blue powder obtained appeared to be hygroscopic. Freshly prepared crystals stored in sealed vials containing mother liquor proved stable for months. Anal. Calcd for $C_{14}H_{18}N_4O_4Cu\cdot2H_2O\cdot CH_3OH$: C, 41.13; H, 5.98; N, 12.80. Found: C, 41.06; H, 5.76; N, 12.98.

**Synthesis of 3.** **1** (0.14 g, 0.46 mmol) was slurried in methanol (40 mL). Distilled 4-pyridinecarboxaldehyde (0.10 mL, 1.0 mmol) was added, and the solution was refluxed for 2.5 h. The reaction mixture was then allowed to cool, and its volume was reduced in vacuo. The solution was stored at room temperature for crystallization, after which the crystalline product was collected by filtration. Upon drying, the crystalline product decomposed to a bright blue powder. A 0.147 g quantity of product was collected (76%). Imino-deuterated complex **3**-*d* was synthesized identically using specifically deuterated aldehyde.[9] Upon storage in the air, the crystalline product decomposed to a bright blue powder over several hours. Freshly prepared crystals stored in sealed vials containing mother liquor proved stable for months. Anal. Calcd for $C_{14}H_{18}N_4O_4Cu\cdot H_2O\cdot CH_3OH$: C, 42.90; H, 5.76; N, 13.34. Found: C, 42.37; H, 5.45; N, 13.77.

**Methylation of 1.** **1-H**$^+$ (0.17 g, 0.5 mmol) was slurried in DMF (10 mL). $Na_2CO_3$ (0.32 g, 0.3 mmol) was added, followed by iodomethane (0.02 mL, 0.3 mmol). The solution was stirred at room temperature for 2 days, after which it was sorbed onto a Sephadex C25 ion exchange column equilibrated with water. The column was then washed with water, causing a blue band to elute; a blue band remained at the top of the column. After repeated washing, the remaining blue band was eluted with $NaClO_4$ (50 mM). The solution was allowed to evaporate to dryness.

**Visible Spectroscopy.** Complex **1-H**$^+$ was studied by titration. A 3.0 mL aliquot of **1-H**$^+$ (3.11 mM) was titrated either with standardized HCl solution (0.0956 M) or with NaOH (0.301 M). Alternately, $Ag_2CO_3$-treated **1-H**$^+$ (0.5 equiv of $Ag_2CO_3$) was titrated with standard $HClO_4$. Complexes **2** and **3** were investigated by using fresh solutions for each pH, due to the instability of the Schiff base linkage at lower pH values.

**Electrochemistry.** Electrochemistry was performed using a hanging mercury drop working electrode and SCE reference electrode in argon-purged 200 mM aqueous phosphate buffer. Scan rates were 5−100 mV/s. 100 mM $NaClO_4$ was included to suppress disproportionation of copper(I). Control samples which lacked $NaClO_4$ exhibited disproportionation but produced midpoint potentials identical to those which contained it. A ∼1.0 mM metal complex concentration was used. Electrochemistry appeared to be reversible, as indicated by linearity of plots of $I$ vs $V^{0.5}$.

**NMR Spectroscopy of Reduced Complexes.** Complexes were prepared in the copper(I) form as follows. Approximately ∼1 mM solutions of complex were dissolved in 100 mM phosphate buffer in $D_2O$ (containing DSS as reference) which had been previously adjusted to the desired pD. Solutions were degassed in a septum-equipped NMR tube with bubbling $N_2$, and the complex was reduced with $Na_2S_2O_4$ under $N_2$. Copper(II) samples were run in $D_2O$ (DSS reference) adjusted to the desired pD.

**Crystallographic Structure Determination of 2.** A blue prismatic crystal of $C_{15.75}H_{27}CuN_4O_{6.75}$ having approximate dimensions of 0.41 × 0.50 × 0.50 mm was mounted on a glass fiber. All measurements were made on a Rigaku AFC6S diffractometer with graphite-monochromated Mo Kα ($\lambda$ = 0.710 69 Å) radiation.

Cell constants and an orientation matrix for data collection, obtained from a least-squares refinement using the setting angles of 16 carefully centered reflections in the range $9.01 < 2\theta < 14.08°$, corresponded to a primitive monoclinic cell with the following dimensions: $a$ = 12.025(8) Å; $b$ = 12.304(5) Å; $c$ = 13.311(8) Å; $\beta$ = 94.76(5)°; $V$ = 1962(1) Å$^3$. For $Z$ = 4 and fw = 443.95, the calculated density is 1.502 g/cm$^3$. The systematic absences of $h0l$, $h + l \neq 2n$, and $0k0$, $k \neq 2n$, uniquely determine the space group to be $P2_1/n$ (No. 14).

The data were collected at a temperature of 23 ± 1 °C using the $\omega-2\theta$ scan technique to a maximum $2\theta$ value of 50.0°. $\omega$ scans of several intense reflections, made prior to data collection, had an average width at half-height of 0.37° with a takeoff angle of 6.0°. Scans of $(1.78 + 0.34 \tan \theta)°$ were made at a speed of 16.0°/min (in $\omega$). The weak reflections ($I < 10.0\sigma(I)$) were rescanned (maximum of four scans), and the counts were accumulated to ensure good counting statistics. Stationary-background counts were recorded on each side of the reflection. The ratio of peak counting time to background counting time was 2:1. The diameter of the incident beam collimator was 1.0 mm, the crystal to detector distance was 285 mm, and the detector aperture was 6.0 × 6.0 mm (horizontal × vertical).

Of the 3696 reflections collected, 3502 were unique ($R_{int}$ = 0.172). The intensities of three representative reflections were measured after every 200 reflections. No decay correction was applied.

The linear absorption coefficient, $\mu$, for Mo Kα radiation is 11.57 cm$^{-1}$. An empirical absorption correction based on azimuthal scans of several reflections was applied which resulted in transmission factors ranging from 0.89 to 1.00. The data were corrected for Lorentz and polarization effects.

The structure was solved by direct methods[10] and expanded using Fourier techniques.[11] Some non-hydrogen atoms were refined anisotropically, while the rest were refined isotropically. Hydrogen atoms were included but not refined. The final cycle of full-matrix least-squares refinement[12] was based on 2046 observed reflections ($I > 3.00\sigma(I)$) and 247 variable parameters and converged (largest parameter shift was 0.02 times its esd) with unweighted and weighted agreement factors of

$$R = \sum||F_o| - |F_c||/\sum|F_o| = 0.049$$

$$R_w = [\sum w(|F_o| - |F_c|)^2/\sum wF_o^2]^{1/2} = 0.045$$

(9) Defoin, A.; Defoin-Straatmann, R.; Kuhn, H. J. *Tetrahedron* **1984**, *40*, 2651.

(10) SIR92: Altomare, A.; Burla, M. C.; Camalli, M.; Cascarano, M.; Giacovazzo, C.; Guagliardi, A.; Polidori, G. *J. Appl. Crystallogr.*, in press.

(11) DIRDIF94: Beurskens, P. T.; Admiraal, G.; Beurskens, G.; Bosman, W. P.; de Gelder, R.; Israel, R.; Smits, J. M. M. *The DIRDIF-94 program system*; Technical Report of the Crystallography Laboratory, University of Nijmegen: Nijmegen, The Netherlands, 1994.

(12) Least-squares: Function minimized was $\sum w(|F_o| - |F_c|)^2$, where $w = 1/\sigma^2(F_o) = [\sigma_c^2(F_o) + (p^2/4)F_o]^{-1}$; $\sigma_c(F_o)$ = esd based on counting statistics, and $p$ = $p$ factor.

The standard deviation of an observation of unit weight[13] was 2.69. The weighting scheme was based on counting statistics and included a factor ($p = 0.010$) to downweight the intense reflections. Plots of $\sum w(|F_o| - |F_c|)^2$ versus $|F_o|$, reflection order in data collection, $(\sin\theta)/\lambda$, and various classes of indices showed no unusual trends. The maximum and minimum peaks on the final difference Fourier map corresponded to 0.70 and $-0.48$ $e/Å^3$, respectively.

Neutral-atom scattering factors were taken from Cromer and Waber.[14] Anomalous dispersion effects were included in $F_c$;[15] the values for $\Delta f'$ and $\Delta f''$ were those of Creagh and McAuley.[16] The values for the mass attenuation coefficients are those of Creagh and Hubbell.[17] All calculations were performed using the teXsan[18] crystallographic software package of the Molecular Structure Corp.

## Results

**Derivatization at the Pendant Amine of 1.** Derivatization of complex **1** to form complexes **2** and **3** was achieved in moderate to high yields by a straightforward Schiff base condensation from the deprotonated complex **1**. Attempts to synthesize complexes from **1**-$\mathbf{H}^+$ in the presence of base failed, possibly due to the interaction of base with the copper center under the conditions of the synthesis. In addition, on the basis of the attempted reactions of the complex with other aldehydes, it appears that an electron-deficient aldehyde favors reaction with **1**. This could be a consequence of the effects of the presence of the copper(II) ion in the vicinity of the site of derivatization.

In addition to Schiff base derivatization at the pendant amine, we have found that **1** can be exhaustively methylated at this position by treatment with iodomethane at room temperature with mild base in DMF. Positively charged products from this reaction were isolated from neutral products by ion-exchange chromatography. Complex **1** has a single primary amine and two secondary amines, all of which could serve as sites for methylation. Since both secondary amines are coordinated to copper, methylation at these amines should cause large changes in the visible spectrum of the complex as compared to the parent complex **1**, while methylation at the primary amine should only cause minor perturbations. As described below, the visible spectrum of the methylated product is very similar to that of **1** (at low pH). This suggests that the preferred site of methylation is at the primary amine.

**$^1$H NMR Studies.** The NMR of the reduced complex **1** (Figure 1a) shows the same features as the spectrum of reduced methylated **1** (Figure 1b). Both spectra show resonances in the normal range for methyl groups (reduced **1**, $\delta$ 1.44, s, 3H; reduced methylated **1**, $\delta$ 1.71, s, 3H). Reduced **1** has a multiplet centered at $\delta$ 3.23 ppm (dd, 4H) and a singlet at $\delta$ 3.62 ppm (4H). The multiplet is assigned to the "linker" methylene units of the six-membered chelate ring of **1**, and the singlet is assigned to the $CH_2^{\alpha}$ methylene groups of the glycine moieties on the basis of chemical shift. This assignment has been confirmed by synthesis of complex **1** with deuterated glycine (not shown).

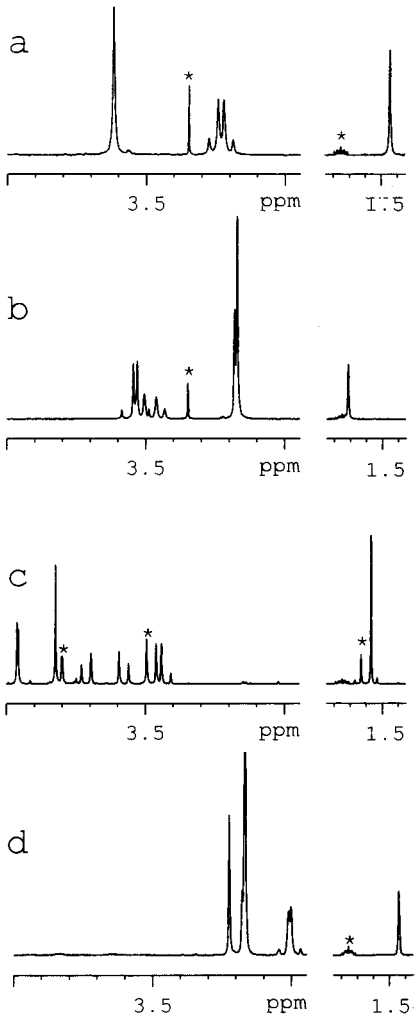


**Figure 1.** 400 MHz $^1$H NMR in $D_2O$ phosphate buffer (pD ~4.5): (a) reduced **1**; (b) methylated reduced **1**; (c) free ligand from **1**; (d) free methylated ligand. Asterisks denote impurity peaks.

The spectrum of reduced methylated **1** (Figure 1b) has two multiplets (at $\delta$ 3.48 (dd, 4H) and 3.54 ppm (dd, 4H)) which are assigned by analogy to the glycine and linker methylene groups. The spectrum of reduced methylated **1** contains additional singlets at $\delta$ 3.17 (6H) and 3.18 ppm (3H), chemical shifts that are typical for alkylamine protons. These are assigned to the protons of the quaternized pendant amine.

The splittings in the spectra of the free ligand of **1** and of the methylated free ligand (Figure 1c,d) are significantly different from those observed for the reduced complexes, indicating that the ligands remain coordinated in the reduced copper(I) species (despite the lack of classically "soft" ligand atoms). The spectrum of the methylated free ligand (Figure 1d) is analogous to the preceding spectra, with the resonance at $\delta$ 1.44 ppm (s, 3H) assigned to the ligand methyl group, the features at $\delta$ 3.01 (dd, 4H) and 3.23 ppm (s, 4H) assigned to the methylene groups, and the resonances at $\delta$ 3.17 (s, 6H) and 3.18 ppm (s, 3H) assigned to the quaternized amine methyls. These appear at the same chemical shift for the free ligand as they do for the metal-complexed ligand (Figure 1b). The chemical shifts of alkylamine protons shift downfield by 0.3−0.6 ppm upon amine coordination to Cu(I),[19−21] so the lack of a chemical shift change for these resonances in the free vs bound state provides

(13) Standard deviation of an observation of unit weight: $[\sum w(|F_o| - |F_c|)^2/(N_o - N_v)]^{1/2}$, where $N_o$ = number of observations and $N_v$ = number of variables.
(14) Cromer, D. T.; Waber, J. T.; *International Tables for X-ray Crystallography*; The Kynoch Press: Birmingham, England, 1974; Vol. IV, Table 2.2 A.
(15) Ibers, J. A.; Hamilton, W. C. *Acta Crystallogr.* **1964**, *17*, 781.
(16) Creagh, D. C.; McAuley, W. J. In *International Tables for Crystallography*; Wilson, A. J. C., Ed.; Kluwer Academic Publishers: Boston, MA, 1992; Vol. C, Table 4.2.6.8, pp 219−222.
(17) Creagh, D. C.; Hubbell, J. H. In *International Tables for Crystallography*; Wilson, A. J. C., Ed.; Kluwer Academic Publishers: Boston, MA, 1992; Vol. C, Table 4.2.4.3, pp 200−206.
(18) teXsan: *Crystal Structure Analysis Package*; Molecular Structure Corp.: The Woodlands, TX, 1985 and 1992.
(19) Van Stein, G. C.; Van Koten, G.; Vrieze, K.; Brevard, C.; Spek, A. L. *J. Am. Chem. Soc.* **1984**, *106*, 4486.

**Table 1.** Crystal Data and Structure Refinement Details for the Structure of 2

| | |
|---|---|
| empirical formula | $C_{15.75}H_{27}CuN_4O_{6.75}$ |
| $D_{calc}$ | 1.502 g/cm$^3$ |
| temp | 23.0 °C |
| radiation | Mo K$\alpha$ ($\lambda$ = 0.710 69 Å), graphite monochromated |
| $\mu$(Mo K$\alpha$) | 11.57 cm$^{-1}$ |
| crystal system | monoclinic |
| unit cell parameters | $a$ = 12.025(8) Å, $b$ = 12.304(5) Å, $c$ = 13.311(8) Å, $\beta$ = 94.76(5)°, $V$ = 1962(1) Å$^3$ |
| space group | $P2_1/n$ (No. 14) |
| $Z$ value | 4 |
| $F_{000}$ | 930.00 |
| no. of reflns measd | total 3696; unique 3502 ($R_{int}$ = 0.172) |
| refln/param ratio | 8.28 |
| residuals:[a] $R$, $R_w$ | 0.049, 0.045 |
| max shift/error in final cycle | 0.02 |

[a] $R = \sum||F_o| - |F_c||/\sum|F_o|$; $R_w = [\sum w(|F_o| - |F_c|)^2/\sum wF_o^2]^{1/2}$.

**Table 2.** Atomic Coordinates and $B_{iso}/B_{eq}$ Values for Non-Hydrogen Atoms of **2**

| atom | $x$ | $y$ | $z$ | $B_{eq}$ |
|---|---|---|---|---|
| Cu(1) | 0.08376(6) | 0.00772(7) | 0.11367(5) | 1.63(2) |
| O(1) | 0.0895(4) | 0.2518(4) | −0.0791(3) | 2.9(1) |
| O(2) | 0.1039(3) | 0.0855(3) | −0.0122(3) | 1.70(10) |
| O(3) | 0.1618(3) | −0.1234(3) | 0.0723(3) | 1.84(10) |
| O(4) | 0.2332(4) | −0.2783(4) | 0.1368(3) | 2.8(1) |
| O(5) | 0.2358(3) | 0.0715(4) | 0.2088(3) | 3.0(1) |
| O(6) | −0.1589(5) | −0.1804(4) | 0.4644(4) | 4.9(2) |
| N(1) | −0.5623(4) | −0.0334(5) | 0.1825(4) | 3.1(2) |
| N(2) | −0.1679(4) | 0.0168(4) | 0.2443(3) | 1.7(1) |
| N(3) | −0.0134(4) | 0.1332(4) | 0.1429(3) | 1.8(1) |
| N(4) | 0.0358(4) | −0.0854(4) | 0.2249(4) | 1.7(1) |
| C(1) | −0.4697(5) | −0.0011(7) | 0.2349(4) | 3.1(2) |
| C(2) | −0.3623(5) | −0.0193(5) | 0.2081(5) | 2.1(1) |
| C(3) | −0.3509(5) | −0.0780(5) | 0.1200(5) | 1.9(2) |
| C (4) | −0.4472(5) | −0.1134(5) | 0.0656(5) | 2.2(2) |
| C(5) | −0.5507(5) | −0.0894(6) | 0.0998(5) | 2.4(2) |
| C(6) | −0.2649(5) | 0.0234(5) | 0.2705(4) | 2.3(2) |
| C(7) | −0.0712(5) | 0.0609(5) | 0.3069(4) | 1.8(1) |
| C(8) | −0.0273(5) | 0.1585(5) | 0.2495(4) | 1.9(1) |
| C(9) | 0.0295(5) | 0.2273(5) | 0.0869(5) | 2.1(2) |
| C(10) | 0.0783(5) | 0.1875(5) | −0.0106(5) | 1.9(2) |
| C(11) | 0.1752(5) | −0.1953(6) | 0.1416(5) | 2.0(2) |
| C(12) | 0.1187(5) | −0.1739(6) | 0.2387(5) | 2.6(2) |
| C(13) | 0.0152(5) | −0.0312(5) | 0.3202(4) | 2.0(2) |
| C(14) | −0.0954(5) | 0.1003(5) | 0.4124(4) | 2.2(2) |
| C(15) | −0.1995(6) | −0.2421(7) | 0.3843(5) | 4.2(2) |

confirmatory evidence that alkylation occurs preferentiallly at the primary amine.

**Description of the Structure of 2.** The expected structure of **2** is confirmed by single-crystal X-ray diffractometry. Crystal data and structure refinement details are summarized in Table 1, and the atomic coordinates are found in Table 2. Table 3 presents selected bond distances and angles for **2**. An ORTEP representation of the structure with the atom-numbering scheme is shown in Figure 2. The structure shows the expected coordination of the metal to the tetradentate ligand forming two five-membered chelate rings with the glycine-derived ligand arms and a six-membered chelate ring bearing the pendant nitrogen. The copper center sits slightly out of the $N_2O_2$ coordination plane by 0.17 Å. This is reflected in the average O(5)−Cu(1)−ligand atom angle of ∼95°. The metal−nitrogen distances average 1.994 Å and are typical for complexes of this type; the parent complex has an identical average M−N length.[8] The metal−oxygen distances average 1.966 Å, also similar to those of the parent complex (1.957 Å).[8] The apical coordination site is occupied by solvent water at a distance of 2.276 Å, suggesting Jahn−Teller distortion. This is slightly shorter than Cu−O(water) bond lengths in a copper macrocyclic amine complex, where a distance of 2.45 Å has been observed.[22] Derivatization at the pendant amine of **1** is confirmed. The Schiff base linkage at this nitrogen exhibits a C−N bond length consistent with double-bond formation [N(2)−C(6) 1.248 Å]. The plane of the pyridine ring is slightly off-center, making an angle of ∼14° with the Cu(1)−C(7) vector. The pyridine nitrogen in the solid state faces away from the unoccupied coordination site. The conformation of the six-membered chelate ring has shifted, as compared to that of the analogous ring in the parent structure **1**-$\mathbf{H}^+$. The nitrogen is equatorial in **1**-$\mathbf{H}^+$ and is axially oriented in **2**.[8]

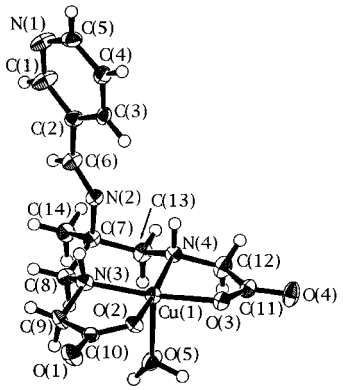


**Figure 2.** ORTEP representation of complex **2** (50% probability ellipsoids). (Solvents of crystallization have been omitted for clarity.)

**Table 3.** Selected Bond Lengths (Å) and Angles (deg) for **2**

| | | | |
|---|---|---|---|
| Cu(1)−O(2) | 1.962(4) | Cu(1)−N(3) | 1.993(5) |
| Cu(1)−O(3) | 1.968(4) | Cu(1)−O(5) | 2.276(4) |
| Cu(1)−N(4) | 1.995(5) | N(2)−C(6) | 1.248(7) |
| O(2)−Cu(1)−O(3) | 93.7(2) | O(2)−Cu(1)−N(4) | 167.9(2) |
| O(2)−Cu(1)−N(3) | 84.5(2) | O(3)−Cu(1)−N(3) | 172.0(2) |
| O(3)−Cu(1)−O(5) | 93.4(2) | O(5)−Cu(1)−N(3) | 94.7(2) |
| O(3)−Cu(1)−N(4) | 84.9(2) | N(3)−Cu(1)−N(4) | 95.1(2) |
| O(5)−Cu(1)−N(4) | 93.1(2) | C(6)−N(2)−C(7) | 121.9(5) |
| O(2)−Cu(1)−O(5) | 99.0(2) | N(2)−C(6)−C(2) | 122.4(6) |

**Electronic Spectroscopy of 1−3.** In the course of studying the solution behavior of **2** and **3**, pH-dependent changes in the electronic spectra of **1**−**3** were observed. These are summarized in Figures 3 and 4, which show the changes in $\lambda_{max}$ of the complexes as a function of pH. There are two significant differences between the spectroscopic pH profiles of the complexes. First, complex **1** has a significantly higher $\lambda_{max}$ value in both the low-pH and high-pH ranges than either **2** or **3**. Second, the wavelength difference between the $\lambda_{max}$ values at the limiting pHs are much larger for **1** (11.6 nm) than for **2** (2.9 nm) or **3** (4.1 nm). The changes for all three complexes occur in the same direction, with higher wavelength $\lambda_{max}$ values at lower pH. The plateau regions of the curves in Figure 3 are similar for complexes **2** and **3** as compared to **1**.

A number of explanations for the origins of the pH-dependent spectroscopic changes shown in Figure 3 are possible. First,

(20) Van Stein, G. C.; Van Koten, G.; Vrieze, K.; Brevard, C. *Inorg. Chem.* **1984**, *23*, 4269.
(21) Van Stein, G. C.; Van Koten, G.; Vrieze, K.; Spek, A. L.; Klop, E. A.; Brevard, C. *Inorg. Chem.* **1985**, *24*, 1367.
(22) Bernhardt, P. V. *J. Chem. Soc., Dalton Trans.* **1996**, 4319.

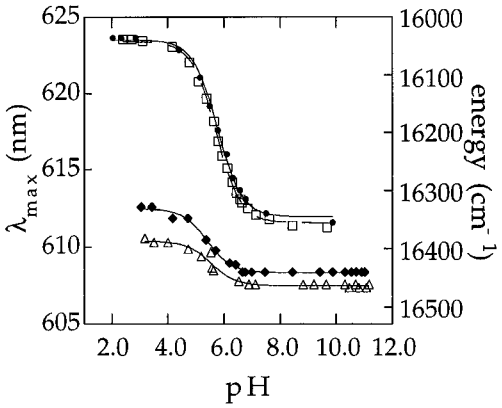


**Figure 3.** pH-dependent spectroscopic shifts in $\lambda_{max}$ for complexes **1**−**3**; ●, $\lambda_{max}$ shifts of **1** with HCl; □, $\lambda_{max}$ shifts of $Ag_2CO_3$-treated **1**-$\mathbf{H}^+$ with $HClO_4$; △, $\lambda_{max}$ shifts of **2**; ◆, $\lambda_{max}$ shifts of **3**. Solid lines represent fits to the equation $(\lambda_{min} + \lambda_{max} \times 10^{pH-pK})/(10^{pH-pK} + 1)$.

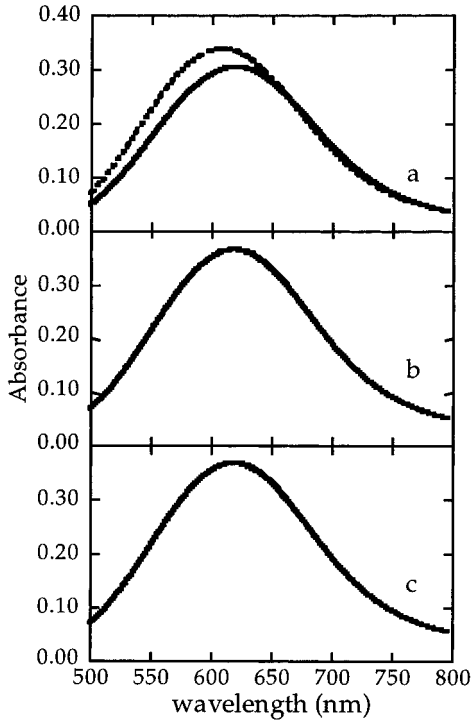


**Figure 4.** Visible spectra in aqueous solution: (a) **1** at pH 8.5 (dashed line) and pH 4.0 (solid line), 5.0 mM; (b) methylated **1** at pH 8.5; (c) methylated **1** at pH 4.0.

complex may dimerize under high-pH conditions, where a deprotonated pendant nitrogen of one complex may coordinate at the apical site of a second complex, with reciprocal coordination of the second complex to the first (Scheme 1a). Second, coordination sphere changes may be involved. Chloride coordination at an axial site could alter $\lambda_{max}$, as pH adjustments were made with HCl. The crystal structure of **1**-$\mathbf{H}^+$ contains an apically coordinated chloride ion.[8] Alternately, $OH^-$ may coordinate axially at high pH, while the aqua ligand is coordinated a lower pH (Scheme 1b). Third, protonation of the pendant nitrogen may alter the affinity for axial ligand coordination ($Cl^-$ or $OH^-$), either by hydrogen bonding between the axial ligand and the ammonium group or by electrostatic interactions. Such ditopic behavior has been described in the cases of nickel(II) complexes[23,24] (Scheme 1c). Finally, the observed shifts in $\lambda_{max}$ may be due exclusively to protonation of the pendant groups and the resulting electrostatic perturbations

**Scheme 1**

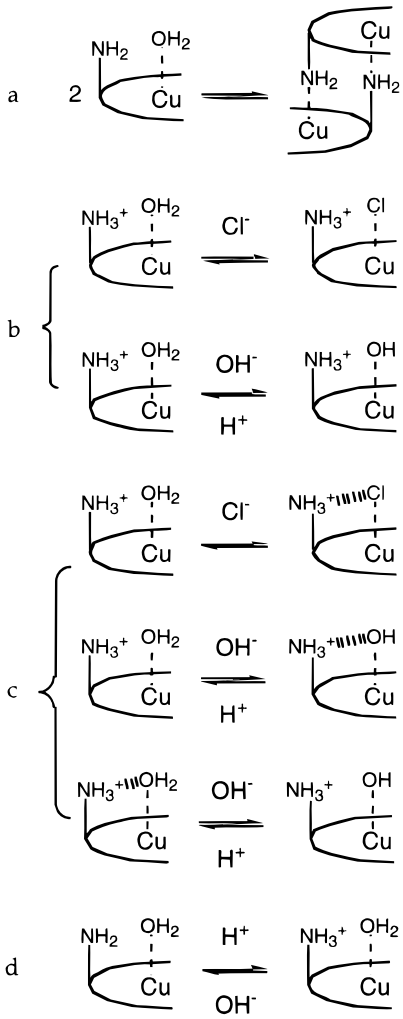


in the complexes and may not involve any coordination sphere changes (Scheme 1d).

To explore these various possibilities, we have examined the spectroscopy of the complexes. The question of metal complex dimerization has been addressed using Beer's-law plots in aqueous solution (pH 7 or 8.5) for all three complexes and in methanol for **2** and **3**. All such plots are linear for **1**−**3**, indicating that dimerization is not likely for any of the complexes (data not shown) in the concentration range studied (≤3 mM). This result is not unexpected for derivatized complexes **2** and **3**, for which dimerization appears unlikely due to steric clashes of the pendant groups. However, **1** may tolerate dimerization well, on the basis of the steric demands of the structure, so the possibility of dimerization of **1** was examined further by EPR spectroscopy. The EPR parameters for complex **1** (12 K, frozen solution) are typical for copper(II) complexes and show no evidence of dimerization at either low or high pH (Table 4). The $g_{||}$ and $A_{||}$ values fall within the standard range for a $N_2O_2$ Cu(II) ligand set[25] and are similar to those of comparable complexes (Table 4). At both limiting pH values, the EPR spectra are nearly identical, confirming that the pH-dependent spectroscopic changes are not due to a

(23) Fabbrizzi, L.; Lanfredi, A. M. M.; Pallavicini, P.; Perotti, A.; Taglietti, A.; Ugozzoli, F. *J. Chem. Soc., Dalton Trans.* **1991**, 3263.
(24) Tsymbal, L. V.; Rosokha, S. V.; Lampeka, Y. D. *J. Chem. Soc., Dalton Trans.* **1995**, 2633.
(25) Peisach, J.; Blumberg, W. E. *Arch. Biochem. Biophys.* **1974**, *165*, 691.

**Table 4.** Spectroscopic Parameters for Complexes **1**−**3**

| complex | $\lambda_{max}$ (nm), ($\epsilon$, $M^{-1}$ $cm^{-1}$) | $g_{\|\|}$ | $g_{\perp}$ | $A_{\|\|}$ ($cm^{-1}$) | ref |
|---|---|---|---|---|---|
| **1**-$H^+$, pH 4.0 | 624 (61.7) | 2.14 | 1.96 | 0.0203 | this work |
| **1**, pH 8.5 | 612 (66.2) | 2.15 | 1.97 | 0.0198 | this work |
| **2**, phosphate buffer, pH 7.0 | 610 (70.7) | | | | this work |
| **2**, methanol | 606 (70.7) | | | | this work |
| **3**, phosphate buffer, pH 7.0 | 610 (72.6) | | | | this work |
| **3**, methanol | 607 (70.5) | | | | this work |
| ((2*S*,8*S*)−2,5,8-methyl−5-nitro−3,7-diaza−2,9-nonanedioato)copper(II) | 598 (*a*) | 2.24 | 2.06 | 0.0194 | 7 |
| ((2*S*,8*S*)−2,8-dibenzyl−5-nitro−3,7-diaza−2,9-nonanedioato)copper(II) | 592 (*a*) | 2.24 | 2.06 | 0.0192 | 7 |

[a] Not given.

**Table 5.** Absorbance Maximum[a] Differences under Low- and High-pH Conditions as a Function of Metal−Pendant Nitrogen Distance for **1**−**3**

| complex | $\lambda_{max}$ (nm) low pH | $\lambda_{max}$ (nm) high pH[b] | energy gap ($cm^{-1}$) | dist (Å)[c] | ref |
|---|---|---|---|---|---|
| **1** | 623.6 | 612.0 | 304 | 4.72 | this work |
| **1**, methylated | 619.6 | 619.6 | 0 | | this work |
| **3** | 612.5 | 608.4 | 110 | 7.71 | this work |
| **2** | 610.4 | 607.5 | 78 | 7.91 | this work |
| (α-*trans*−6,13-dimethyl−6,13-bis(dimethylamino)-1,4,8,11-tetraazacyclotetradecane)copper(II) | 522 | 497 | 964 | 3.85[d] | 22 |
| (*β*-*trans*−6,13-dimethyl−6,13-bis(dimethylamino)-1,4,8,11-tetraazacyclotetradecane)copper(II) | 529 | 508 | 781 | 4.80 | 22 |

[a] $\lambda_{max}$ values determined from first-derivative spectra. [b] pH ≥ 7. [c] Values for **2** and **3** based on the crystallographic structure of **2**. We have used the crystallographic values, assuming that rotation about the N(2)−C(7) bond is slow relative to the experimental time scale, due to steric hindrance between the secondary amine hydrogens and the Schiff base moiety. [d] Cambridge Crystallographic Data Centre.[33]

monomer−dimer equilibrium. Therefore, it appears that dimerization of any of the complexes is not a viable explanation for the pH-dependent spectroscopic changes.

We examined the second possible explanation, that of coordination of axial ligands, by treating the complexes with different ligands. Since HCl was used to adjust the solution pHs, axial chloride coordination is a possible source of the changes. Addition of chloride concentrations of up to 1 M NaCl caused no perturbation in the *d*−*d* absorbances of any of the complexes, as compared to the spectra of chloride-free solutions (data not shown). Conversely, removal of all chloride from **1** by treatment with the $Ag^+$ ion followed by titration with $HClO_4$ led to a spectroscopic pH profile essentially identical with that found for titration with HCl (Figure 3). Since these two ligands differ significantly in affinity and ligand field splitting in aqueous solution, it is unlikely that they would produce identical $\lambda_{max}$ values at all pHs studied, as is observed. Therefore, it appears that simple axial coordination is not a tenable explanation for the observed spectroscopic shifts.

The possibility of coordination of $OH^-$ as the source of spectroscopic perturbation is more difficult to assess. To explore further the role of hydroxide ion, we have exhaustively methylated the pendant amine of **1**. This removes the protonation equilibrium of the pendant amine as a factor in the observed spectroscopic changes. In the range of pH 4−8 (pH adjustments with NaOH and $HClO_4$), the electronic spectra of methylated **1** are unchanged, with $\lambda_{max}$ at 620 nm, very close to the $\lambda_{max}$ of 624 nm found in the low-pH region with underivatized **1** (Figure 4). This result appears to rule out explanations involving simple axial coordination of the hydroxo ligand to **1**, which is equivalent to titration of an axially coordinated water. With regard to **2** and **3**, if simple axial hydroxide ion coordination is responsible for the spectroscopic changes, then the size of the changes should be similar for **1**−**3**, contrary to our observation. This appears to contradict axial $OH^-$ coordination as an explanation.

The third type of explanation, which involves ditopic effects between a coordinating axial ligand interacting with a protonated pendant group. The axial ligand may be either the chloride or the hydroxide ion, as above. The interaction of the axial ligand with the pendant protonated nitrogen that stablilizes coordination may either be hydrogen bonding in nature or electrostatic. A ditopic effect does not seem likely for **1** (whether hydrogen bonding or electrostatic in nature), because the pH dependence using HCl is superimposable on that found using $HClO_4$. Given the difference in characteristics between these two ligands, it is improbable that they would exhibit identical ditopic features. The presence of a ditopic effect involving $OH^-$ is more difficult to rule out. On the basis of the results obtained with methylated **1**, a ditopic effect with $OH^-$ that is purely electrostatic in nature can be eliminated; however, one that involves hydrogen bonding from the axial hydroxo ligand to the pendant amine cannot be.

The final explanation, in which the entire effect is attributed to changes in the electrostatic field of the molecule upon protonation of the pendant nitrogen, is also consistent with the data presented above. In this case, the presence of a full charge on the pendant nitrogen alters d-orbital energies and potentially alters transition moment dipoles, relative to those of the deprotonated state. A through-space electrostatic effect such as this should be inversely dependent on distance. The energies of the observed shifts are consistent with this picture, with the energy gap between low- and high-pH absorbance maxima falling with increasing distance between metal center and pendant nitrogen, as shown in Table 5. On the basis of our data, we cannot distinguish between this explanation and a ditopic effect involving $OH^-$. For this reason, we have not extracted $pK_a$ values from the data in Figure 3, since it is not clear if a single group is being protonated or if the effect represents the combination of two protonation events.

**Protonation Site of Complexes.** The site of protonation of complexes **2** and **3** was investigated by $^1H$ NMR. Both **2** and **3** exhibit paramagnetically broadened $^1H$ NMR resonances.

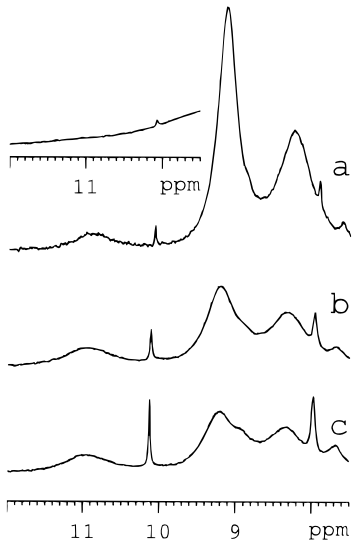


**Figure 5.** $^1$H NMR spectra of complex **3** in $D_2O$ solution: (a) **3** at pD 8.6 (inset: **3**-*d* at pD 8.6); (b) **3** at pD 7.7; (c) **3** at pD 7.2. Narrow peaks are ascribed to partial hydrolysis at lower pD.

**Table 6.** Electrochemical Parameters[a] from Cyclic Voltammetry for **1**−**3**

| | $E_{1/2}$ (mV) | | |
|---|---|---|---|
| complex | low-pH range[b] | high-pH range[c] | $\Delta E_{1/2}$ (mV) |
| **1** | −249 | −390 | 141 |
| **2** | −275 | −379 | 104 |
| **3** | −283 | −383 | 100 |

[a] All potentials vs SCE. [b] pH 4.0. [c] pH 8.5 for **1** and pH 7.0 for **2** and **3**.

Figure 5a shows the aromatic region of **3** (pD 8.6). Three resonances are observed, which are tentatively assigned on the basis of intensity to the two sets of aromatic protons ($\delta$ 8.26 and 9.15 ppm) and the Schiff base proton of the complex ($\delta$ 10.9 ppm). These assignments are confirmed by the spectrum of Schiff base-deuterated **3**-*d* (Figure 5a, inset) and the lack of any resonances in this region for the parent complex **1** (not shown). Upon lowering of the solution pD to ∼7.7 (Figure 5b), the resonance at $\delta$ 8.26 ppm shifts to slightly lower field and the resonance at $\delta$ 9.15 ppm splits, showing a new resonance at $\delta$ 9.21 ppm. When the pD is lowered further to 7.2 (Figure 5c), both changes become more pronounced. The Schiff base proton appears unaffected by these changes in pD, although the broadness of this resonance may hide subtle effects. Complex **2** behaves similarly (data not shown). We interpret these data as implying that the site of protonation for **2** and **3** is the pyridine nitrogen and not the Schiff base nitrogen.

**Electrochemistry.** Cyclic voltammetry on **1**−**3** in aqueous solution (phosphate buffer) exhibited reversible behavior between −100 and −500 mV. Cyclic voltammagrams showed a ∼60 mV splitting. This is consistent with the NMR data presented above, which indicate that the metal complex remains intact during the Cu(II)/Cu(I) redox cycle. Table 6 contains the midpoint potentials for **1**−**3** at low and high pH and the corresponding $\Delta E_{1/2}$ values. The $E_{1/2}$ values at low pH become more positive compared to their high pH positions. The direction of these shifts is consistent with stabilization of the reduced state by a proximate positive charge. Presumably, this reflects a stabilization of the electroactive orbital in these $d^9$ complexes. An analogous observation has been made for a series of ferrocene derivatives bearing pendant amines, where positive shifts in midpoint potential were observed for the complexes bearing pendant ammonium groups vs those bearing amines.[5] In this work, a linear relationship between the difference in midpoint potentials between the ammonium-bearing and the amine-bearing complexes and the inverse of the metal−nitrogen distance, was observed. This relationship is not apparent in our data; however, it may be obscured by experimental error.

## Discussion

The pH-dependent electronic spectra discussed above (Figure 3) have a number of features worthy of comment. The similarities in overall behavior of **2** and **3** vs **1** suggest that the structure of **3** is analogous to that of **2** and differs similarly from the structure of **1**. The origins in the differences of **2** and **3** vs **1** likely lie in structural variations between the two sets of complexes. The structural variations involved may consist of slight differences in the $N_2O_2$ coordination geometry between the parent complex **1** and the derivatized complexes. The average metal−nitrogen distances are identical for the two complexes, but the metal−oxygen distances are slightly longer for **2** than for its parent **1** (0.01 Å). However, this difference is inadequate to explain the variances in $\lambda_{max}$ between **1** and **2** (and **3** by inference), since its size is small, and **2** would be expected to have a smaller ligand field splitting than **1** by this criterion (its $\lambda_{max}$ values are consistently at higher energy).

A likelier explanation for the observed spectroscopic differences is found in the conformation of the six-membered chelate rings of the complexes, which places the pendant exocyclic nitrogen either in an equatorial (as in **1**) or an axial (as in **2**) position. The effects of this conformational difference have been explored by Bernhardt through isolation and structural characterization of both the axial (denoted α) and equatorial (denoted $\beta$) isomers of (*trans*-6,13-dimethyl-6,13-bis(dimethylamino)-1,4,8,11-tetraazacyclotetradecane)copper(II), which contain chelate rings of the same type as **1**−**3**.[22] The $\Delta\lambda_{max}$ of the isomers ($\Delta\lambda_{max} = \lambda_{max}^{equatorial} - \lambda_{max}^{axial} = \lambda_{max}^{\beta} - \lambda_{max}^{\alpha}$) is 7 nm at low pH and 11 nm at neutral pH.[22] This pattern is similar in size and direction of shift to that of the complexes described here, where the $\Delta\lambda_{max}$ of the complexes ($\Delta\lambda_{max} = \lambda_{max}^{equatorial} - \lambda_{max}^{axial} = \lambda_{max}^{1} - \lambda_{max}^{2or3}$) is ∼14 nm (**2**) and ∼12 nm (**3**) in the low-pH range and ∼4 nm (**2**) and ∼3 nm (**3**) in the high-pH range. A detailed analysis of the effect by Bernhardt indicated that the shift in $\lambda_{max}$ is not due to any substantial differences in the coordination of the chelate ring to the metal between the two isomers but rather due to hydrogen bonding between the exocyclic nitrogen in the α-isomer and the metal-coordinated secondary nitrogens of this complex, an arrangement which is geometrically inaccessible for the $\beta$-isomer.[22] By analogy, the same hydrogen-bonding effect appears to occur in complexes **2** and **3**, between the Schiff base nitrogen and the secondary amines of the complexes, although in the present cases, the Schiff base nitrogens must serve as hydrogen-bond acceptors and not donors as in the examples characterized by Bernhardt.

The complexes studied by Bernhardt also exhibit a pH-dependent shift in visible $\lambda_{max}$ similar to that reported in this study.[22] The pH-dependent shift in $\lambda_{max}$ for Bernhardt's α-isomer (neutral solution vs 0.1 M HCl) is 25 nm, and the shift for the $\beta$-isomer 21 nm; these values are about twice that found for complex **1** (assuming that the pH transition is complete at pH 7 for Bernhardt's compounds as for **1**−**3**. The directions of the shifts are the same as those found for **1**−**3**, with the higher wavelength absorbance appearing at low-pH conditions. These values are compared to values for complexes **1**−**3** in Table 5. Bernhardt has attributed the observed shifts to a ditopic effect

involving axial $Cl^-$ ligation.[22] On the basis of our comparison of the behavior of **1** in the presence of $Cl^-$ to its behavior with $ClO_4^-$, it appears that a ditopic effect involving $Cl^-$ is ruled out in our system. This, in addition to the differences in the sizes of the shifts, may simply reflect the fact that complex **1** (and **2** and **3** by analogy) differs electronically and chemically from the isomeric examples of Bernhardt.[22]

The data presented in this study suggest that the spectroscopic and electrochemical shifts in $\lambda_{max}$ that are observed for complexes **1**−**3** either are due to the a ditopic effect between an axially coordinated aqua/hydroxide ligand and the pendant amine of complexes **1**−**3** or are due purely to the electrostatic effect created by the presence of a charged group at a distance and orientation restricted by covalent attachement to the ligand. Even if a ditopic effect occurs in **1**−**3**, it will involve a protonation of pendant nitrogen and axial hydroxo ligand. The resulting change in charge will constitute a significant electrostatic contribution to the measured spectroscopic and electrochemical changes.

A naive picture of the ligand field splitting of complexes **1**−**3** suggests that a ditopic effect involving hydrogen bonding of axial $OH^-$ can be ruled out. Since the aqua ligand generally falls above the hydroxo ligand in the spectrochemical series,[26] the ligand field splitting at low pH, as indicated by the $\lambda_{max}$, should be larger than that in the high-pH range. As shown in Figure 3, the high-pH-range $\lambda_{max}$ values are consistently at higher energy. If this simple picture is correct, then the pH-dependent changes observed would be solely due to the electrostatic changes in the complex as a function of pH. We note that the behavior of methylated **1**, which fixes the electrostatic interaction at the pendant nitrogen, has a spectrum at both low and high pH ($\lambda_{max} = 620$ nm) that is nearly identical with that found in the low-pH spectrum ($\lambda_{max} = 624$ nm) of **1** (Table 5). The difference between the two may reflect a slight difference in the conformation of the chelate ring involved, or it could reflect the lack of a ditopic hydrogen-bonding interaction to an axial ligand. These results, however, appear to support the notion that the majority of the effect causing the 12 nm spectroscopic shift from high to low pH is electrostatic in origin.

Even if the simple picture is not entirely correct, the absorbance energies of the protonated complexes decline relative to those of the deprotonated species in all cases (Table 5). The electrochemical data indicate a stabilization of the electroactive orbital at low pH, and a similar argument can be applied to the other d orbitals. However, the decline of the absorbance peak energies with pH suggests that the ligand field splittings diminish in this process, so the d orbitals are apparently unequally affected by protonation of the complex. Thus, the presence of a pendant charged group creates a collapse of the d orbital manifolds of all three complexes. On the basis of the behavior of methylated **1**, we attribute this effect largely to the electrostatic effects in the complexes and less to coordination sphere changes. In the small sample of molecules presented in this study, the extent of the collapse correlates well with distance between pendant nitrogen and copper center, assuming that rotation about the N(2)−C(7) bond is slow relative to the experimental time scale (due to steric hindrance) and that the solid-state distances from the crystallographically determined structures of **1**[8] and **2** are generally representative of the equilibrium metal−nitrogen distances. However, factors other than distance are likely involved, on the basis of the following consideration. Presumably, one of the key parameters for both electronic spectroscopy and electrochemistry is the interaction of the pendant charge with the HOMO. In the case of first-row transition elements, the HOMO probably has a dominant d-orbital contribution. It may be that the interaction of the charged group with the HOMO has an angular dependence in addition to a distance dependence, on the basis of the location of the orbital nodes. For those orbitals where the charged group lies on or near the node, any effects are expected to be less, compared to the cases where the charge interacts with the electron density maximum of the orbital lobe. Thus, the angle of the charged group off the normal to the equatorial coordination plane may have an influence on the pH-dependent changes described here. The differences in the distance dependencies of spectroscopic shifts for the complexes listed in Table 5 may be due to different angular dependencies superimposed on a distance dependence.

Perturbations in electrochemical behavior have been observed for a variety of metalloproteins which bear ionizable groups proximate to the metal site. These changes in midpoint potential have been effected by titration of protonatable groups, as in azurins[27] and pseudoazurin,[28,29] or by placement of charged residues through site-directed mutagenesis, examples of which are myoglobin,[30] cytochrome $b_5$,[31] and cytochrome $c$.[32] The effects of proximate charges on metalloprotein chromophores have not been studied to the same extent as have electrochemical perturbations. The examples of structurally characterized model complexes that exhibit pH-dependent spectroscopic and electrochemical changes described here should help shed light on the distance and angular dependencies of the effects and should help elucidate whether similar effects occur in metalloproteins.

**Acknowledgment.** We acknowledge the University of Connecticut Research Foundation for partial support of this work and Prof. H. Frank and Dr. V. Chynwat for their assistance in obtaining the EPR spectra.

**Supporting Information Available:** Tables of atomic coordinates and $B_{eq}$ values, anisotropic displacement parameters, and bond distances and angles for non-hydrogen and hydrogen atoms of complex **2** (10 pages). Ordering information is given on any current masthead page.

IC9703843

(26) Cotton, F. A.; Wilkinson, G. *Advanced Inorganic Chemistry*, 4th ed.; J. Wiley & Sons: New York, 1980; Chapter 20.

(27) Strong St. Clain, C.; Ellis, W. R., Jr.; Gray, H. B. *Inorg. Chim. Acta* **1992**, *191*, 149.

(28) Dennison, C.; Kohzuma, T.; McFarlane, W.; Suzuki, S.; Sykes, A. G. *Inorg. Chem.* **1994**, *33*, 3299.

(29) Sakurai, T.; Ikeda, O.; Suzuki, S. *Inorg. Chem.* **1990**, *29*, 4715.

(30) Varadarajan, R.; Zewert, T. E.; Gray, H. B.; Boxer, S. G. *Science* **1989**, *243*, 69.

(31) Rodgers, K. K.; Sligar, S. G. *J. Am. Chem. Soc.* **1991**, *113*, 9419.

(32) Komar-Panicucci, S.; Bixler, J.; Bakker, G.; Sherman, F.; McLendon, G. *J. Am. Chem. Soc.* **1992**, *114*, 5443.

(33) Allen, F. H.; Kennard, O. *Chem. Des. Automat. News* **1993**, *8*, 1, 31.